Sea Ice Detection and Measurement Using Coastal GNSS Reflectometry: Analysis and Demonstration

Feng Wang ⓘ, Dongkai Yang ⓘ, Mingjie Niu, Lei Yang ⓘ, and Bo Zhang ⓘ

Abstract—Based on a developed three-layer air–ice–water reflection model, this article simulates the evolution of reflection coefficient versus elevation angle. Due to the interference between the signal components from the air–ice and ice–water interfaces, the reflection coefficient experiences an oscillating pattern versus elevation angle so that detecting sea ice using the power or amplitude of the reflected global navigation satellite system (GNSS) signal has to choose a suitable satellite to reduce the influence of the oscillating pattern. A sea ice surface is more stable and presents higher correlation than a dynamic ocean surface, this article explores the potential of detecting and measuring sea ice using the coherency of reflected GNSS signal for coastal scenario. Experimental results show that phase coherency can significantly detect sea ice without strictly limiting elevation and azimuth angle. This article also is to is to explore the potential of retrieving sea ice thickness using the oscillating phase pattern versus elevation angle. The phase compensation and the dual-polarization observation are proposed to remove the delay phase between the direct and reflected signal from the estimated phase of the reflected GNSS signal. The results show that the amplitude and frequency of the oscillating phase pattern, respectively, have an inversely proportional and positively linear relationship with sea ice thickness. Simulation shows that, compared to the oscillating amplitude, the oscillating frequency is a better choice to measure sea ice thickness. The frequency of the dual-polarization oscillating pattern could provide the measurement performance with a root-mean-square error of 0.05 m.

Index Terms—Coastal global navigation satellite system-reflectometry (GNSS-R), correlation time, dual-polarization observation, phase compensation, random walk test, sea ice detection, sea ice thickness.

I. Introduction

SEA ICE has a significantly important influence on monitoring climate change. In addition, the risk of sea ice disaster directly affects human activities, such as marine transportation, safe production of oil, and gas resources. Due to the importance of monitoring climate and human development, it is necessary to detect and measure sea ice. Optical imaging [1] is an usual way to detect and measure sea ice, however, it is easily affected by weather, such as clouds, rain and fog so that it is incapable of detecting sea ice all-weather and all-day. Compared to optical imaging, microwave remote sensing, such as synthetic aperture radar (SAR) [2], passive radiometers [3], altimeters [4], and scatterometers [5] have also been used to detect and measure sea ice. Radiometers and scattermeters have typically 25–50 km resolution, which is low. SAR and altimeters have high spatial resolution, however, are difficult to use for high temporal-resolution detection and measurement due to high costs and power requirements.

Since GNSS signals reflected off the earth's surface were proposed to explore earth's physical parameters [6], [7], global navigation satellite system reflectometry (GNSS-R) has been applied to various remote sensing of earth's physical parameters, such as sea surface height [8], wind speed [9], soil moisture [10], vegetation [11]. As a bistatic or multistatic configuration, it is low-power, low-cost and can simultaneously receive the signals from different GNSS satellites to offer the observation with the high spatial and temporal resolution.

GNSS-R also affords an opportunity for the detection and measurement of sea ice. The first demonstration of sea ice remote sensing using GNSS-R was conducted by an aircraft experiment [12]. In [13], the theoretical reflection of GPS signals from ice sheet was investigated and then airborne and spaceborne measurements were simulated. The results indicated that the reflected GPS signals are sensitive to snow surface roughness and firn parameters. The permittivity and roughness from different sea ice types were obtained from the waveforms of the reflected GPS signals in [14]. The UK Disaster Monitoring Constellation (UK DMC) mission first presented the capability of GNSS-R in global remote sensing of sea ice from spaceborne platforms [15]. After that, the UK TechDemoSat-1 (TDS-1) and Cyclone GNSS (CYGNSS) promoted the rapid development of spaceborne GNSS-R in sea ice remote sensing [16], [17]. For sea ice measurement of GNSS-R, some works have been done for sea ice concentration [18], [19], ice sheet [20], sea ice altimetry [21], and ice thickness [22] using UK TDS-1 data. At present, new sea ice measurements also have been demonstrated. In [23], the sensitivity of the reflected GNSS signals to sea ice types was demonstrated and a multistep classification was proposed

Feng Wang, Dongkai Yang, Mingjie Niu, and Bo Zhang are with the School of Electronic and Information Engineering, Beihang University, Beijing 100191, China (e-mail: wangf.19@163.com; yangdongkai@sina.com; 13621339799@163.com; bozhang@buaa.edu.cn).

Lei Yang is with the School of Information Science and Engineering, Shandong Agricultural University, Taian 271018, China (e-mail: yanglei@sdan.edu.cn).

to distinguish young ice, first-year ice and multiyear ice in Arctic sea. The capability of GNSS-R for Greenland ice sheet melt was investigated using TDS-1 data in [24]. Multiangular and multi-frequency method has been proposed to retrieve simultaneously sea ice and snow thickness [25].

Spaceborne remote sensing is difficult for the sea ice near the coastline due to coarse resolution. In addition, it is also important for safe production to detect and measure sea ice around oil rigs in real time. Therefore, long-term and reliable observation from the coastline or oil rigs is important for both climate monitoring and safe production. Coastal experiments have for example been conducted in Greenland [26] and Bohai Bay of China [27]. In [28] the method of detecting sea ice using single-antenna GNSS-R was proposed and demonstrated by an experiment. For sea ice measurement of coastal GNSS-R, few works have been started for sea ice altimetry [29], and sea ice thickness [30], [31]. Although some works have been done using coastal GNSS-R to detect and measure sea ice, there are two shortcomings. On the one hand, existing works ignored the role of sea water on which the signals penetrating sea ice occur the reflection, especially in the case of thin ice; on the other hand, except for sea ice altimetry, the phases of the reflected GNSS signals rarely were explored and used to detect and measure sea ice. Actually, the phases of the reflected GNSS signals have the potential to detect and measure sea ice [21].

This article evaluates the capability of detecting sea ice and measuring ice thickness using the phase of the reflected GNSS signals. Because a GNSS signal can penetrate sea ice and a reflection occurs on the ice–water interface, a three-layer re-flection model is developed. The interferometric amplitudes and phases of the GNSS signals reflected off sea ice and sea water are discussed. The correlation time and a random walk test are used to explore the feasibility of detecting sea ice using the coherency of the reflected GNSS signals. Furthermore, for different sea ice thickness, the phases of the GNSS signals reflected off sea ice show different oscillating phenomenon which can be used to retrieve sea ice thickness. Section II gives the model of the GNSS reflected signals off sea ice and the explanation of the interference phenomenon between the signal components from the air–ice and ice–water interface. Methods of detecting sea ice using the phase coherency of the reflected GNSS signal are described in Section III. Section IV describes the experiment of detecting sea ice and analyzes the experimental results. The potential of retrieving sea ice thickness is discussed in Section V. Finally, Section VI concludes this article.

II. MODEL OF GNSS SIGNAL REFLECTED OFF SEA ICE

A. Geometry of Surface Reflection

Fig. 1 sketches the three-layer reflection model including air, sea ice and sea water. Due to a low dielectric difference between air and sea ice, GNSS signals partially are reflected by the air–ice interface, and the remainders penetrate through the sea ice to the ice–water interface and then occur the reflection. The components reflected off the air–ice and ice–water interface coherently superpose in air to produce the totally reflected
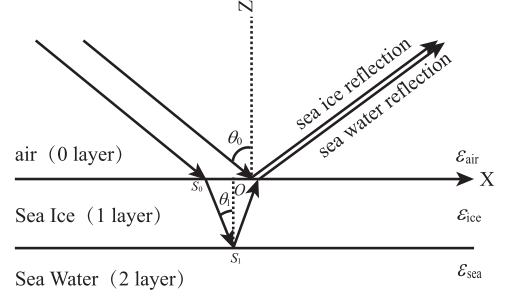

Fig. 1. Three-layer model including air, sea ice, and sea water.

signals. Interference between the signal components from the two interfaces could be expected.

B. Permittivity

The relative permittivities of sea water and ice depend on their temperature and salinity. The relative permittivity of sea water could be computed by the Debye expression as [32]

$$\varepsilon_{\text{sea}} = \varepsilon_\infty + \frac{\varepsilon_s - \varepsilon_\infty}{1 + (j2\pi f\tau)^{1-\alpha}} - j\frac{\sigma}{2\pi f\varepsilon_0} \tag{1}$$

where f is the signal frequency; ε_∞ is the dielectric constant at infinite frequency; ε_s is the static dielectric constant; τ is the relaxation time in seconds; σ is the ionic conductivity; α is an empirical parameter that describes the distribution of relaxation time; and ε_0 is the permittivity of free space 8.854×10^{-12}. The detailed definition and computation are given in [32]. For a signal with 1 GHz frequency, the relative permittivity of the sea ice is modeled as [33]

$$\varepsilon_{\text{ice}} = \varepsilon_{\text{ice0}} + (0.009 + j0.005)\, V_b \tag{2}$$

where $\varepsilon_{\text{ice0}}$ is the relative permittivity of pure ice and is $3.12 + j0.04$; V_b is the relative brine volume which was given in [34] as

$$V_b = 10^{-3} S_{\text{ice}} \left(-\frac{49.183}{T_{\text{ice}}} + 0.532 \right) \tag{3}$$

where S_{ice} and T_{ice} are the salinity and temperature of sea ice. In [35], through analyzing Arctic sea ice data, S_{ice} and sea ice thickness approximately agree with a piecewise function as

$$S_{\text{ice}} = \begin{cases} 14.24 - 19.39 h_{\text{ice}} & h_{\text{ice}} \le 0.4 \text{ m} \\ 7.88 - 1.59 h_{\text{ice}} & h_{\text{ice}} > 0.4 \text{ m} \end{cases} \tag{4}$$

where h_{ice} is sea ice thickness in meter. From (4) it is seen that as sea ice thickness increases, sea ice salinity decreases. This is to say that compared to first year (30 to <200 cm) and multiyear ice (>200 cm), new (<10 cm) and young ice (10 to <30 cm) retain high salinity values. When the temperature and salinity of sea water are respectively 2 °C and 20‰, the permittivity of sea ice is $79.35 + j \cdot 33.04$, and for sea ice, when the temperature and sea thickness are respectively −2 °C and 2 m, the permittivity is $3.13 + j \cdot 0.046$. Compared to sea water, sea ice permittivity has lower difference with that of the air so that a GNSS signal penetrates through sea ice and a reflection occurs on the ice–water interface for thin sea ice.

C. Reflection Coefficient

The right- and left-hand circular polarization (R and LHCP) reflection coefficients are expressed as

$$\Gamma_{R(L)} = \Gamma_{R(L)01} + \Gamma_{R(L)12}e^{j2h_{ice}\alpha} \tag{5}$$

$\Gamma_{R(L)01}$ and $\Gamma_{R(L)12}$ are the reflection coefficients of the air–ice and ice–water interface, and expressed as

$$\Gamma_{R(L)01} = \frac{\Gamma_{\perp 01} \pm \Gamma_{\parallel 01}}{2} \tag{6}$$

$$\Gamma_{R(L)12} = \frac{T_{\perp 10}\Gamma_{\perp 12}T_{\perp 01} \pm T_{\parallel 10}\Gamma_{\parallel 12}T_{\parallel 01}}{2} \tag{7}$$

where $\Gamma_{\perp ij}$ and $\Gamma_{\parallel ij}$ are the vertical polarization and horizontal polarization reflection coefficients of the interface between the ith and jth layer, respectively; $T_{\perp ij}$ and $T_{\parallel ij}$ are the vertical polarization and horizontal polarization transmission coefficients from the ith to jth layer, respectively; α is expressed as

$$\alpha = k_{air} \cdot \sin\theta_1 \sin\theta_0 - \frac{k_{ice}}{\cos\theta_1} \tag{8}$$

where k_{air} is the wave number of the air, i.e., $2\pi f\sqrt{\varepsilon_{air}}$; k_{ice} is the wave number of the ice, i.e., $2\pi f\sqrt{\varepsilon_{ice}}$; θ_0 and θ_1 are the incident angle of the signal to the air–ice and ice–water interface, respectively. The detailed derivation of the reflection coefficient is presented in Appendix A. The vertical and horizontal polarization reflection coefficients are expressed as

$$\Gamma_{\perp i,i+1} = \frac{\eta_{i+1}\cos\theta_i - \eta_i\cos\theta_{i+1}}{\eta_{i+1}\cos\theta_i + \eta_i\cos\theta_{i+1}} \tag{9}$$

$$\Gamma_{\parallel i,i+1} = \frac{\eta_i\cos\theta_i - \eta_{i+1}\cos\theta_{i+1}}{\eta_i\cos\theta_i + \eta_{i+1}\cos\theta_{i+1}} \tag{10}$$

where η_i is the impedance of the ith layer. The vertical and horizontal polarization transmission coefficients are expressed as [36]

$$T_{\perp i,i+1} = \frac{2\eta_{i+1}\cos\theta_i}{\eta_{i+1}\cos\theta_i + \eta_i\cos\theta_{i+1}} \tag{11}$$

$$T_{\parallel i,i+1} = \frac{2\eta_{i+1}\cos\theta_i}{\eta_i\cos\theta_i + \eta_{i+1}\cos\theta_{i+1}}. \tag{12}$$

Fig. 2 gives the changing trends of the RHCP and LHCP reflection coefficients as elevation angle increases for different sea ice thickness through simulating using (5). For the RHCP reflection coefficient, regardless of sea ice thickness, as elevation angle increases, the amplitude of the reflection coefficient decreases and has no significant oscillating pattern, and the phase shows an oscillating pattern around 0°. As shown in Fig. 3(a), the reason is that the wave components from the ice–water interface are lower than 20% of the total RHCP waves so that it has small impact on the reflected RHCP wave. The amplitude and phase of the LHCP reflection coefficient appear different for different sea ice thickness. When sea ice thickness is 0.1 m, the amplitude and phase both monotonically increase as elevation angle increases. The amplitude and phase both oscillate for sea ice thickness above 0.5 m, and the thicker the sea ice thickness is the faster the amplitude and phase oscillate. The total LHCP waves reflected
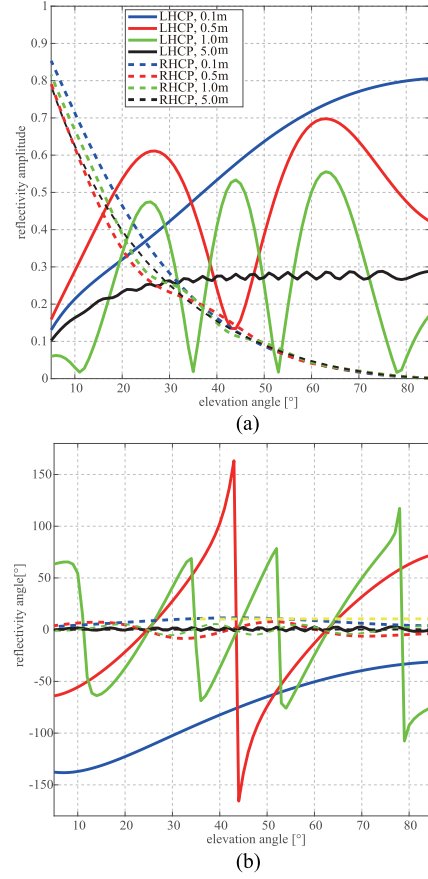

Fig. 2. Simulated relationship between (a) amplitude and (b) phase of RHCP and LHCP reflection coefficients and the elevation angle of GNSS satellites for different sea ice thickness.
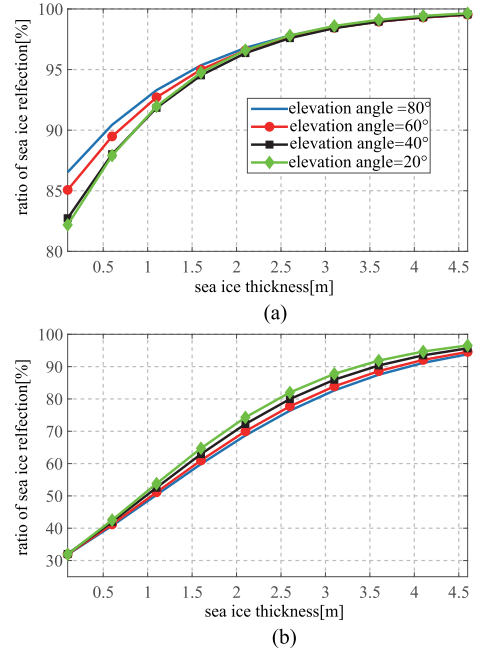

Fig. 3. Simulated percentage of the wave components from the air–ice interface versus sea ice thickness.

to air are the coherent superposition of the signals reflected off the air–ice and ice–water interface. Two reflected LHCP waves produce interference so that when the phase difference of the two waves is $n \cdot \pi + \pi/2$, the two LHCP waves interfere constructively, and when the phase difference is $(n+1) \cdot \pi$, two waves interfere destructively. For the case of 0.1 m sea ice thickness, the varying range of the phase difference of two LHCP waves is smaller than $\pi/2$ when the elevation angle increases from $5°$ to $85°$, therefore, the amplitude and phase pattern of the LHCP reflection coefficients do not show any oscillation, but a monotonic change as a function of elevation angle. As shown in Fig. 3(b), as sea ice thickness becomes thicker, the attenuation of the waves in the ice layer increases, and the wave component from the ice–water interface weakens so that the oscillation pattern gradually fades. In the case with the sea ice less than 1 m, the wave components from the ice–water interface is more than 50% of the total LHCP waves. This is the reason why in [22] the reflection of the air–ice interface is neglected to derive the model for retrieving sea ice thickness, but with increasing sea ice thickness the derived model produces more noticeable model errors. The amplitude oscillation pattern as a function of elevation angle has been found when the amplitude of the reflected signal from dry snow was analyzed in [37]. From the reflection coefficient pattern as a function of elevation angle, two conclusions could be obtained. One is that this oscillation pattern impacts sea ice detection using the observables computed simply from the amplitude of the reflected signal. The other is that it is possible to detect and measure sea ice using this oscillation pattern. This oscillating pattern has been found and used to retrieve sea ice and snow thickness in the MOSAiC experiment in which a sequence retrieval approach based on nonlinear least square was proposed [25].

The reflection coefficient for an ice slab also can be computed as [34]

$$\Gamma_{\perp(\|)} = \frac{\Gamma_{\perp(\|)01} + \Gamma_{\perp(\|)12}e^{-2jk_{\mathrm{ice}}h_{\mathrm{ice}}}}{1 + \Gamma_{\perp(\|)01}\Gamma_{\perp(\|)12}e^{-2jk_{\mathrm{ice}}h_{\mathrm{ice}}}}. \tag{13}$$

Here, we demonstrate the equivalence of the two models. Fig. 4 shows the changing trends of the reflection coefficient amplitude and angle as elevation angle increases for the two models. It is clear that the reflection coefficients of the two models are equivalent.

D. Model of Reflected GNSS Signal

Assuming that the GNSS signal experiences coherent reflection, the total received waveform could be

$$Y_p(\tau) = T_i\sqrt{P_r}\Gamma_p\Lambda(\tau - \Delta\tau)e^{-j\frac{2\pi\Delta\tau}{\lambda}} \tag{14}$$

where T_i is the coherent integration time; P_r is expressed as

$$P_r = \frac{\lambda^2 G_t P_t G_r}{(4\pi)^2(R_t + R_r)^2} \tag{15}$$

where λ is the signal wavelength; G_t and P_t are the transmitted power and transmitting antenna gain, respectively; R_t and R_r are the distance from GNSS satellite and receiver to the specular reflection point, respectively. $\Delta\tau$ is the delay between
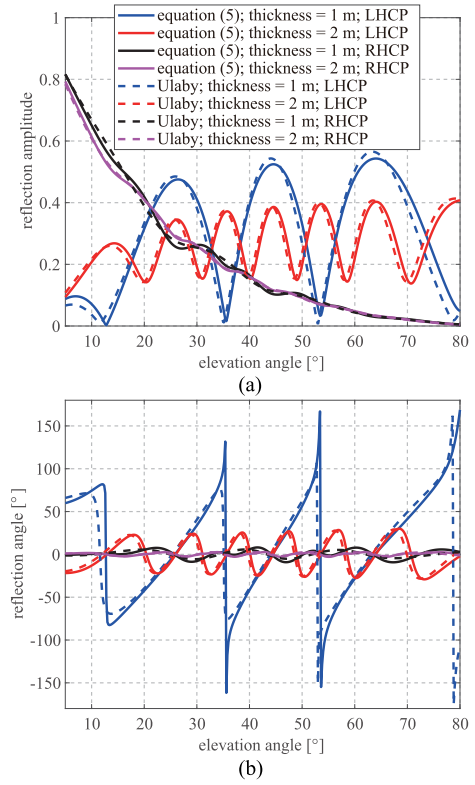

Fig. 4. (a) Simulated reflection amplitude and (b) angle versus elevation angle for two reflection coefficient models.

TABLE I
PARAMETERS OF SIMULATED SCENARIO

parameter	unit	value
GNSS satellite height	km	20200
transmitted power	w	26.8
transmitting gain	dB	12.1
receiving gain	dB	12
signal bandwidth MHz		1.023
code type	-	Gold
elevation angle	°	5∼85
receiver height	m	10
receiver beam width	°	±30
receiver point angle	°	45

the reflected and direct signals, and for a coastal scenario is expressed as

$$\Delta\tau = \tau_r - \tau_d = \frac{2h\cos\theta_0}{c} \tag{16}$$

where h is the receiver height relative to sea ice surface and c is the light speed.

Fig. 5 shows the amplitude and phase of the reflected signal versus elevation angle for the scenario as given in Table I. In Fig. 5(a), it is clear that due to the modulation of the receiving antenna gain pattern, the amplitude oscillation patterns of the reflected signal are different with these of the reflection coefficients. In addition, GNSS signals usually experience noncoherent scattering on the ice-free sea surface [38]. The reflection coefficients, the receiving antenna gain modulation and the noncoherent scattering on sea water surface all influence the ability to distinguish between sea ice and water. It is necessary
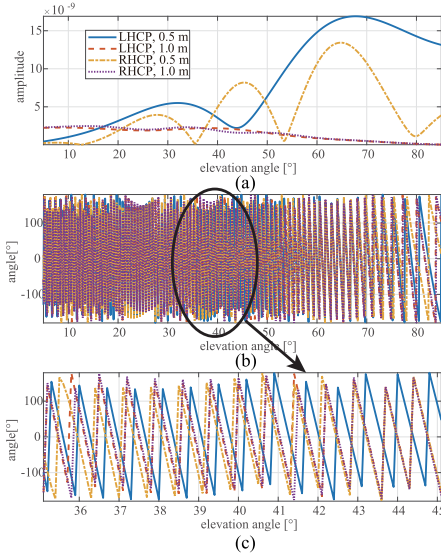
Fig. 5. Simulated (a) amplitude, (b) phase, and (c) zoomed phase of reflected GNSS signal for the scenario of Table I.

to explore the phase coherency of the reflected signal to detect and measure sea ice. Compared to the irregular oscillation of the signal amplitude, as presented in Fig. 5(b) and (c), the phases of the reflected signal show regular periodic oscillation. Unlike the amplitude oscillation pattern of the reflection coefficient, the oscillation ranges of the signal phases is relatively stable and is independent on the sea ice thickness. Furthermore, the oscillation pattern of the reflected signal phase is faster than that of the amplitude. In fact, the phase oscillation of the reflected signal contains two oscillating types. One is a slow oscillation caused by the changing reflection coefficient versus elevation angle. The other is a fast oscillation caused by the time-varying delay between the reflected and the direct signal, for which the oscillating frequency depends on the receiver height relative to sea ice surface as

$$f_o = \frac{1}{2\pi} \frac{\partial \left(4\pi h \cos \theta_0 / \lambda \right)}{\partial \theta} = \frac{2h}{\lambda} \sin \theta_0. \tag{17}$$

To measure sea ice using the phase of the reflected signal, it should be necessary to compensate the phase caused by the delay between the reflected and the direct signal.

III. DETECTION OF SEA ICE

At present, the method to detect sea ice mainly is using the amplitude of the reflected GNSS signal, such as the power ratio of the reflected and direct signal [27], and the polarimetric ratio of the reflected RHCP and LCHP signal [14], [29].

A. Amplitude Method

1) Power Ratio: The ratio of the reflected and direct signal is expressed as

$$R_{rd} = \frac{P_{rL}}{P_d} = \frac{\left\langle |Y_{rL\,\max}|^2 \right\rangle - N_{rL}}{\left\langle |Y_{d\,\max}|^2 \right\rangle - N_d} \tag{18}$$

where $\left\langle |Y_{rL\,\max}|^2 \right\rangle$ and $\left\langle |Y_{d\,\max}|^2 \right\rangle$ are the waveform peaks of the reflected LHCP signal and direct signal, respectively; N_{rL} and N_d are the floor noise of the reflected LHCP signal and direct signal, respectively, which are computed by averaging the power in the signal-free waveform.

2) Polarimetric Ratio: The polarimetric ratio of the reflected RHCL and LHCP signal is defined as

$$R_{LR} = \frac{P_{rL}}{P_{rR}} = \frac{\left\langle |Y_{rR\,\max}|^2 \right\rangle - N_{rR}}{\left\langle |Y_{rL\,\max}|^2 \right\rangle - N_{rL}} \tag{19}$$

where $\left\langle |Y_{rR\,\max}|^2 \right\rangle$ and N_{rR} are the peak and floor noise of the waveform of the reflected RHCP signal, respectively. As mentioned above, the amplitude of the reflected signal shows an oscillating pattern as a function of elevation angle, therefore, when using the amplitude of the reflected signal to detect sea ice it is necessary to choose the signals from suitable satellites to reduce the impact of the reflection coefficient oscillation and the antenna modulation due to the changing elevation angle. In this article, the phase coherency of the reflected signal will be explored to detect sea ice to avoid choosing the signals from suitable satellites.

B. Phase Method

The phase coherency of the reflected signal has been used in retrieving significant wave height [39], wind speed [40], sea correlation time [41], and inland water [42]. For the actual surface, the reflection has a specular component which is coherent and a diffuse one which is incoherent [43]. When the surface is smooth, such as the most of sea ice surface, the specular component dominates, and on contrary for a rough surface, such as the most of sea surface, the diffuse, or incoherent component dominates. The coherency of the reflected GNSS signal has been found to be proportional to the presence of sea ice using experimental data [45]. In this article, the correlation time and a random walk test are used to detect sea ice.

1) Correlation Time: In [39] and [46], the interferometric complex field (ICF) is defined as

$$S_{\mathrm{icf}}(t) = \frac{I_{rp}(t) + jQ_{rp}(t)}{I_d(t) + jQ_d(t)} \tag{20}$$

where $I_{rp}(t) + jQ_{rp}(t)$ and $I_d(t) + jQ_d(t)$ are the complex correlation values at the waveform peak of the reflected and direct RHCP or LHCP (represented by symbol p in above equation) signal, respectively. The direct signal is used to remove the features unrelated to surface characterization, such as residual Doppler, direct signal power and navigation message. To estimate the correlation time, the autocorrelation function of the ICF is defined as

$$R(\Delta t) = \frac{1}{T_{\mathrm{int}}} \int_0^{T_{\mathrm{int}}} S_{\mathrm{icf}}(t) \cdot S_{\mathrm{icf}}^*(t - \Delta t) \, dt \tag{21}$$

where T_{int} is the integration time. The correlation time is defined as the width of the autocorrelation function

$$\tau_{\mathrm{icf}} = \frac{\int_0^{+\infty} R(\Delta t) \, d\Delta t}{R(0)}. \tag{22}$$
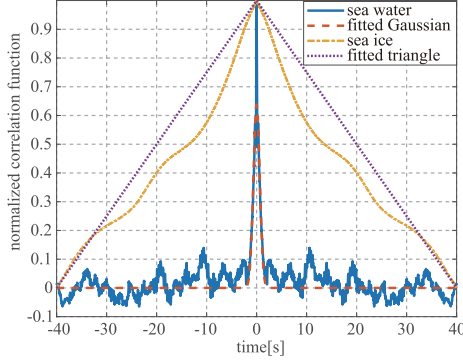
Fig. 6. Autocorrelation function of ICF of GNSS signals reflected off the sea water and ice surface, and corresponding fitted curves using Gaussian and triangle functions. The acquired GNSS signal is from the Bayuquan experiment.

Fig. 7. Simulated relationship between correlation time of sea water and wind speed using (24) and (26).

When the surface height is assumed to have a gaussian probability distribution, the autocorrelation function of the ICF can be approximated by a Gaussian function as [39]

$$R_{\text{sea}}(\Delta t) \approx A(h_{\text{swh}}, l_z, \theta_0, G_r) e^{-\frac{(\pi h_{\text{swh}} \cos \theta_0 \Delta t)^2}{2(\lambda \tau_z)^2}} \quad (23)$$

where h_{swh} is the significant wave height, l_z is the surface autocorrelation length, and τ_z is the surface correlation time. An example for the normalized autocorrelation function of the actual data and the fitted Gaussian function are shown in Fig. 6, indicating a good agreement. The correlation time of sea water is approximately expressed as [39]

$$\tau_{\text{icf}} \approx \frac{\lambda}{\pi} \left(\frac{a_s}{h_{\text{SWH}}} + b_s \right) \quad (24)$$

where a_s and b_s are 0.167 and 0.388. Considering fully developed sea, the wind-wave relationship is modelled by the well-known Pierson–Moskowitz spectrum as

$$SWH \approx 0.22 \frac{U_{10}^2}{g} \quad (25)$$

where g is the gravity acceleration; U_{10} is the 10-m wind speed. In [41], the correlation times using coastal GNSS-R data have also an inversely proportional relationship with wind speed as

$$\tau_{\text{icf}} = 3 \frac{\lambda}{U_{10}} \text{erf} \left(2.7 \frac{\rho}{U_{10}^2} \right) \quad (26)$$

where $erf(\cdot)$ is the error function; ρ is the resolution of the observed pixel. For wind speed below 12 m/s, the relationship is approximated as $\tau_{\text{icf}} = 3 \frac{\lambda}{U_{10}}$. Fig. 7 gives the correlation time of sea water as wind speed increases, in which when wind speed is over 1.5 m/s, the correlation times from the two models are both below 500 ms, and when wind speed is lower than 1.5 m/s, the two models deviate each other. Equation (24) considers the influence of the elevation angle, and for the same sea condition as elevation angle increases the correlation time decreases. When wind speed and elevation angle are 0.5 m/s and 30°, respectively, the correlation time is 3.64 s. When elevation angle or wind speed go to 0, the correlation times go to infinity. This strong coherency in reflected signals for low elevation-angle case has been used in GNSS-IR to retrieve earth's parameters [44]. It
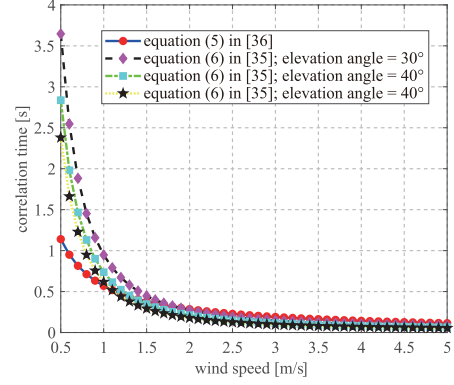
should be noted that at low wind speed, due to the influence of other sea parameters, such as swell, the actual correlation time may be lower than the modelled correlation time in (24) and (26). For most sea conditions and observation geometries the correlation time of sea water is on the level of a few hundred milliseconds. The same results were obtained from experiment data in [40] in which when wind speed ranges from 0 to 25 m/s, the correlation time varies between 0 and 150 ms.

An ice surface is stable and the signals reflected off an ice surface present very high correlation time. For a smooth surface, the reflected signal is modeled by (14) and the ICF is expressed as $\sqrt{P_r} \Gamma_p e^{-j \frac{2\pi \Delta \tau}{\lambda}} \sqrt{P_d}$. In the integration time, the delay between the reflected and the direct signal $\Delta \tau$ is assumed to be a constant, and the autocorrelation function of the ICF is written by a typical "triangle" function as

$$R_{\text{ice}}(\Delta t) = \frac{P_r |\Gamma_p|^2}{T_{\text{int}} P_d} (|\Delta t| + T_{\text{int}}). \quad (27)$$

As shown in Fig. 6, due to the nonspecular reflection caused by the roughness of the sea ice surface and the volume scattering in the ice layer, the actual autocorrelation function differs from the theoretical model, however, it is far wider than that of the signal reflected off the ice-free sea surface. Therefore, it is possible to detect sea ice using the correlation time of the reflected signal. When the correlation time is larger than a given threshold, sea ice is considered to be present. It should be noted that for the case with very low elevation angle or very clam sea surface, the signal reflected off the sea surface may also present high correlation time. It is desirable to exclude the reflected signals with low elevation angle, such as the signals with the elevation angle lower than 30°, and make the reflector height as high as possible. In addition, sea state changes faster than sea ice state, therefore, long-time or time-sequence observations can reduce the risk of error discrimination.

2) Random Walk Test: For a GNSS signal, when the ice-free sea surface is reasonably rough, the waves over glistening zones will shift the wave phase randomly so that the phase of the reflected signals appear randomly fluctuating [47]. However, the phase of a reflected signal from sea ice surface presents relative regularity. Here, the randomness of the time-series phase of the reflected signal will be used to detect sea ice. The phase
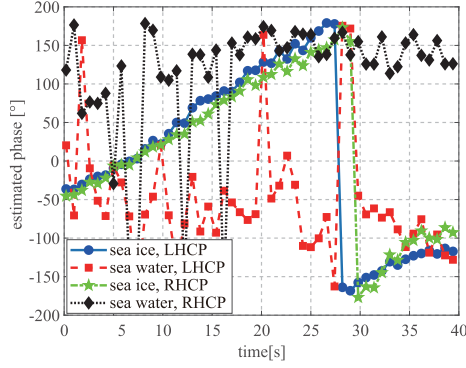
Fig. 8.   Estimated phases of the signals reflected off ice-free sea surface and sea ice surface, respectively. The acquired GNSS signal is from the Bayuquan experiment.

of the reflected signal is defined as

$$\widehat{\varphi}_p = \operatorname{atan2}\left(\frac{Q_{rp}}{I_{rp}}\right). \tag{28}$$

Fig. 8 presents the estimated phases of the signals reflected off an ice-free sea surface and a sea ice surface. It is clear that the phases of the signal reflected off ice-free sea surface appear more random than these of the signals reflected off sea ice.

Here, a random walk test [48] is used to measure the randomness of the time-series phase. The details of the random walk test are the following:

1) Compute the median of the sequence, and divide the sequence into two types: the elements of the type 1 are larger than the median and the ones of the type 2 are smaller than the median;
2) count the elements of type 1 and the element of type 2, which are, respectively, named as $n1$ and $n2$;
3) map the elements of the type 1 to 1 and the elements of the type 2 to 0 to produce a new sequence;
4) compute the number of the runs of the new sequence r;
5) compute the test statistic z as

$$z = \frac{r + 0.5 - 1 - 2n_1 n_2 n}{\sqrt{2n_1 n_2 \left(2n_1 n_2 - n\right)\left[n^2\left(n - 1\right)\right]}}. \tag{29}$$

A random sequence has a higher run number than a regular one, therefore the run number could be used to distinguish between sea ice and sea water. For a two-sided test, when $|z| \geq z_{\alpha/2}$ (where $z_{\alpha/2}$ is the quantile of significance level α), the sequence is considered to be random. Therefore, the test statistic z is also an important index for the randomness of the sequence and may also be utilized to detect sea ice.

IV. EXPERIMENT FOR SEA ICE DETECTION

A. Scenario

The experiment of sea ice detection was conducted at the Bayuquan Ocean Observatory (40.283°N, 122.092°E) in Yingkou of the Chinese Liaoning province. The experiment scenario and the antenna setup are shown in Fig. 9. The antennas' height relative to the sea surface is about 20 m. Directional RHCP
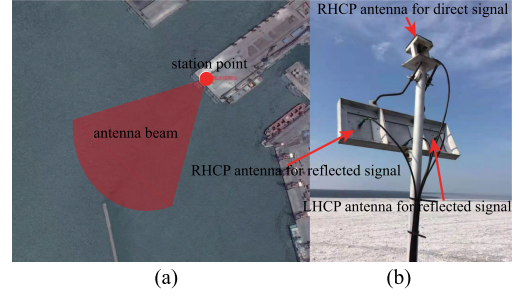

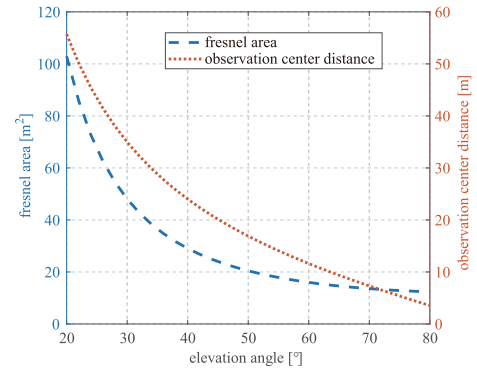Fig. 9.   (a) Aerial view of experiment scenario and (b) antenna setup in the experiment.

Fig. 10.   Computed Fresnel area and horizontal distance from the observation center to the antenna phase center versus elevation angle for the Bayuquan experiment.

and LCHP antennas with a gain of 13 dB and a beam width $\pm 20°$ were used to receive reflected GPS L1 signal. The signals from the satellites with the elevation angle from $25°$ to $65°$ and the azimuth from $210°$ to $250°$ could be received. The experiment was carried out in two stages including a sea ice period from January 15 to 17, 2016 and an ice-free water period at March 24, 2016. The used device in the experiment was a two-channel collector with the intermediate frequency, the sampling frequency and the quantization of 3.996 MHz, 16.369 MHz, and 2 b. The experiment data were intermittently acquired every 30 minutes and each data file contains about 50-second of the direct and reflected GNSS signals. The corresponding temporal resolution can be considered as 30 min. There was weak wind speed, and the sea surface experienced low dynamics during the experiment so that the reflected signal from the sea surface presents high coherence.

The coherent signal mainly comes from the first Fresnel zone. The spatial resolution is determined by the geometry, but not by the surface roughness [49]. As shown in Fig. 10, as the elevation angle increases, the Fresnel area and the horizontal distance from the observation center to the antenna phase center decrease. When the elevation angle is $20°$, the spatial resolution and the observation distance are considered as about 102.92 m^2 and 55.71 m, respectively, and for the elevation angle of $80°$, the spatial resolution and observation only are 12.36 m^2 and 3.54 m, respectively.
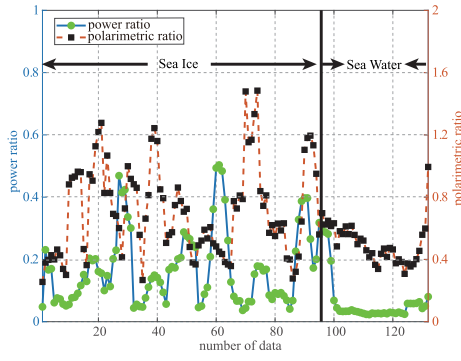
Fig. 11. Power ratio and polarimetric ratio of the signals reflected off sea ice and ice-free sea surface in the Bayuquan experiment.

Fig. 13. Correlation time of the signals reflected off sea ice and ice-free sea surface in the Bayuquan experiment.
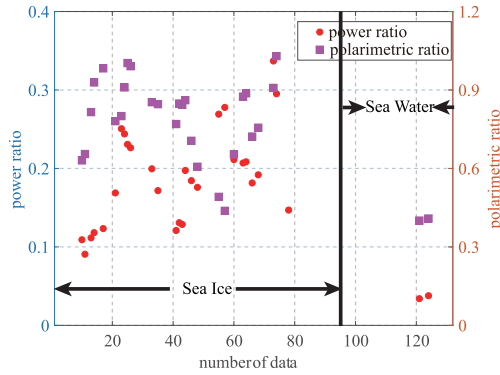

Fig. 12. Power ratio and polarimetric ratio of the signals reflected off sea ice and ice-free sea surface for limited elevation and azimuth angle in Bayuquan experiment.

Fig. 14. Run numbers of the phase sequences of the reflected signal off sea ice and ice-free sea surface in the Bayuquan experiment.

B. Results

Fig. 11 gives the power and polarimetric ratio defined by (18) and (19) for sea ice and ice-free surface. It is clear that the power and polarimetric ratio for sea ice show a lot of fluctuation. As analyzed in Section II, this fluctuation is mainly caused by the interference between the reflected signal components from the air–ice and ice–water interface. For the ice-free sea water the power and polarimetric ratio are relative steady. It should be noted that due to the modulation of the antenna pattern for different directional signals and discontinuous acquisition for the reflected signals, the power and polarimetric ratio show large fluctuations, therefore, when the elevation angle and azimuth angle are not limited, it is impossible to distinguish between sea ice and sea water. When the elevation angle is limited from $45°$ to $65°$, and the azimuth angle is limited from $180°$ to $300°$, as shown in Fig. 12, the power ratio and polarimetric ratio can distinguish between sea ice and sea water, and the fluctuations for sea ice are significantly weaker than without limiting the elevation and azimuth angle. However, the total number of sampling points for the detection process reduces to 23% of the total number of observations.

Fig. 13 shows the correlation time of the signals reflected off sea ice and ice-free sea water. It is seen that the correlation time for sea ice is larger than 12 s and the averages are 15.33 s and 14.99 s for the LCHP and RCHP signals. However, the
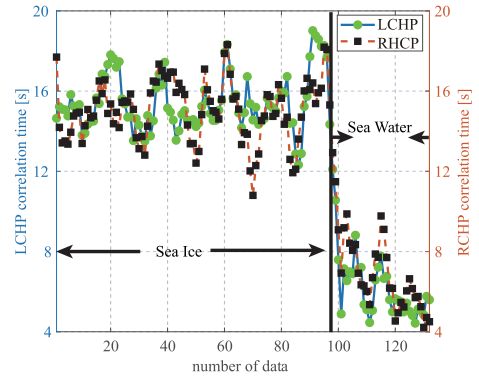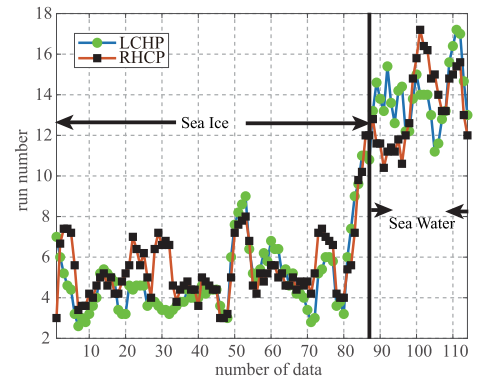
correlation times for ice-free sea water are mostly between 4 s to 10 s and, with the average values of 6.09 s and 6.84 s. Thus, it is possible to distinguish between sea ice and sea water based on the correlation time of the reflected signal. Compared to the power and polarimetric ratio, it is not necessary to strictly limit the elevation and azimuth angle. The correlation time can use all experimental data to detect sea ice.

As shown in Fig. 14, the run number of the phase sequences for sea ice is from 2 to 8, and the averages are both 5 for the LCHP and RCHP signals. However, the averaged run number of the phase sequences for ice-free sea is 13. Compared to sea ice, different surface height and orientations over the glistening zone will randomly shift the phases of reflected signal. The test statistic z for sea ice and ice-free sea surface are given in Fig. 15, in which the test statistic for sea ice is below -3.5, and the averages are -5.01 and -4.85 for the LCHP and RCHP signals. However, for the LCHP and RCHP signal reflected off ice-free sea the averaged test statistics are -2.22 and -2.32, respectively. These results show that the randomness of the reflected signal could be used to detect sea ice.

Compared to the amplitude of the reflected signal, the methods based on the phase of the reflected signal can detect sea ice without selecting suitable satellites and calibrating the uncertainty factor such as antenna pattern.
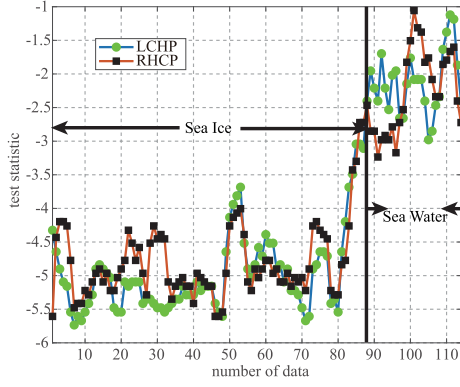
Fig. 15. Test statistic z of the phase sequences of the signals reflected off sea ice and ice-free sea surface in Bayuquan experiment.

Fig. 16. Retrieved height and truth versus different sea ice thickness for the simulation scenario of Table I.

V. POTENTIAL OF RETRIEVING SEA THICKNESS

Because of the penetration of the GNSS signals into sea ice, the altimetric residual between the retrieved height and MSS has been found to be consistent with sea ice thickness [21]. This result indicated the potential of retrieving sea thickness using the phase of the reflected signal. The methods of retrieving sea ice thickness using the oscillating phase pattern are explored to further demonstrate this potential. As shown in (14) the phase of the reflected signal is jointly determined by the reflection coefficient and the delay between the reflected and the direct signal. Therefore, to use the oscillating phase pattern to retrieve sea ice thickness, the first step is to remove the delay phase from the estimated phase of the reflected signal. In addition, defining the features sensitive to sea ice thickness from the oscillating phase pattern is also important to measure sea ice thickness.

A. Phase Compensation Method

A method for removing the delay phase between the reflected and the direct signal is using the estimated delay from the (16) to compensate. For this method it is necessary to know the antenna height relative to the sea ice surface. As shown in (17), the oscillating frequency of the time-varying delay phase is proportional to the antenna height. From Fig. 5(b) and (c), it is seen that the phase pattern of the reflected signal mainly presents a fast oscillation of the delay phase. Therefore, the oscillating pattern of the reflected signal versus elevation angle is used to retrieve the antenna height relative to sea ice surface. The first step is to create the time-series vector $(x_i, y_i) = (4\pi \sin\theta\lambda, \widehat{\varphi}_p)$; and then to estimate the spectrum of the created time-series vector using the Lomb–Scargle method [50]; finally, to obtain the spectrum peak which is the retrieved height.

Fig. 16 gives the retrieved height and the truth versus different sea ice thickness for the simulation scenario of Table I. When sea ice thickness is below 1 m, due to the influence of the signals from the ice–water interface, the retrieved heights experience a large bias, and the evolution of the bias is in good agreement with sea ice thickness. However, in case of sea ice thickness above 1 m, because of the decreasing influence of the reflection on the ice–water interface as shown in Fig. 3(b), the retrieved heights are gradually close to the truth. The delay between
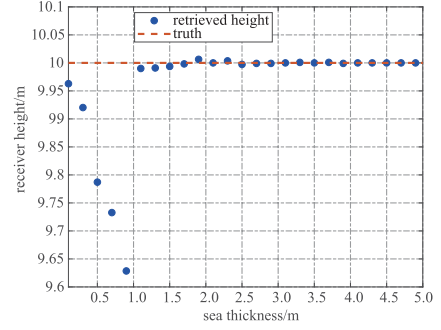
the reflected and the direct signal is computed using (16) and then the compensated phase $\Delta\hat{\varphi}_{rd}$ is derived as $2\pi\Delta\tau/\lambda$. As shown in Fig. 2(b), the oscillating amplitude and frequency of the reflection coefficient phase pattern are relative to sea ice thickness, therefore, the following observable is defined as:

$$M(\theta) = \cos\left(\hat{\varphi}_L(\theta) - \Delta\hat{\varphi}_{rd}(\theta)\right). \tag{30}$$

A least square fit between the defined observable and the cosine function is used to estimate the oscillating amplitude and frequency of the defined observable as

$$\left\{\widehat{a}, \widehat{b}, \widehat{c}\right\} = \underset{\{a,b,c\}}{\arg\min}\left\{\left|M(\theta) - a\cos(b\cdot\theta + c)\right|^2\right\} \tag{31}$$

where a, b, and c are the fitted parameters. a and b, respectively, represent the amplitude and frequency of the oscillating pattern.

B. Dual-Polarization Observation

Reflected LCHP and RHCP signal go through the same geometric delay path, therefore, the dual-polarization observation could be used to remove the delay phase. The observable is defined as

$$M(\theta) = \cos\left(\widehat{\varphi}_L(\theta) - \widehat{\varphi}_R(\theta)\right) \tag{32}$$

where $\hat{\varphi}_L(\theta)$ and $\hat{\varphi}_R(\theta)$ are the phase of the reflected LCHP and RHCP signal, respectively. Least squares fitting as shown in (31) is used to estimate the oscillating amplitude and frequency of the defined observable.

Through simulation, the relationships between the amplitude and frequency of the defined observable and sea ice thickness are obtained. As shown in Fig. 17, the oscillating frequency has a linear relationship with sea ice thickness for sea ice thickness from 0 to 5 m. However, when sea ice thickness is below 1 m, the oscillating amplitude remains 1, and when sea ice thickness is above 1 m, the oscillating amplitude is dropping as sea ice thickness increases. With increasing sea ice thickness, the sensitivity of the oscillating amplitude to sea ice thickness decreases. This will result in a more serious retrieval error for thicker sea ice. The oscillating frequency does no show this phenomenon because of a linear relationship. This indicates that the oscillating frequency is a better choice than the oscillating amplitude to measure sea ice thickness. The relationships between sea ice thickness and the amplitude and frequency of the defined oscillating pattern
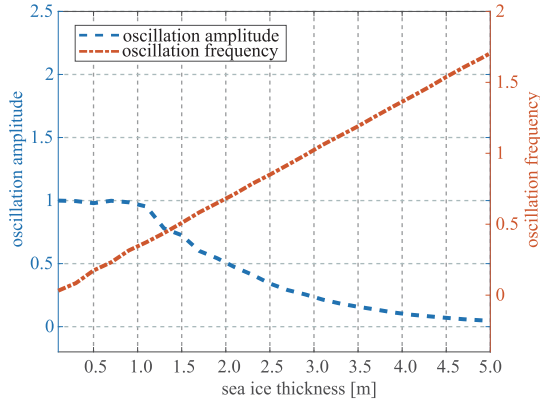
Fig. 17. Simulated relationships between the amplitude and frequency of the observable defined by (32) and sea ice thickness. The simulated scenario is given in Table I.

are approximated as

$$h_{\text{ice}} = \sum_{i=0}^{N} p_i \cdot obs^i \tag{33}$$

where obs represents the amplitude and frequency of the defined oscillating pattern; p_i is the polynomial coefficient; and N is the order number of the polynomial, here for the amplitude is 3 and for frequency is 1.

C. Influence Factors

Sea ice temperature, sea water salinity, and sea water temperature also determine the reflection coefficient so that they may affect the retrieval of sea ice thickness. As shown in Fig. 18, the simulation shows that sea ice temperature has no significant influence on the oscillating frequency, however, as sea ice temperature increases, the oscillating amplitude increases, and for the thicker sea ice, this increasing trend is more obvious. Through analyzing the influence of sea water temperature and salinity on the oscillating amplitude and frequency of the defined observable, it is found that they have no significant impact on the oscillating pattern. This is to say that sea ice temperature, sea water temperature and salinity all have no significant influence on the retrieval of sea ice thickness using the oscillating frequency of the defined observable. This is the other reason why the oscillating frequency is a better choice than the oscillating amplitude to retrieve sea ice thickness.

D. Simulation Test

Here, Monte Carlo simulation is used to analyze and evaluate the measurement performance of retrieving sea ice thickness using the proposed methods and observable. The simulation procedure is as follows:

1) Randomly generate 13 000 sea ice thicknesses for the scenario as given in Table I;
2) simulate RHCP and LHCP waveforms for the above sea ice thicknesses using the models expressed by (14) and (15), and then add gaussian noise to simulated waveforms;
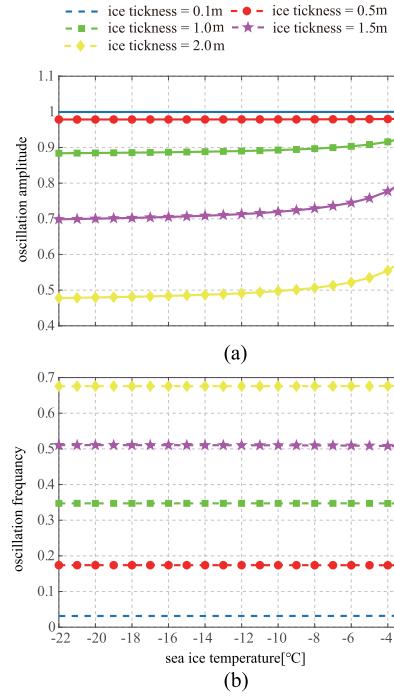

Fig. 18. Simulated influence of the sea ice temperature on oscillating (a) amplitude and (b) frequency of the observable defined by (32) for different sea ice thickness. The simulated scenario is given in Table I.

3) compute the oscillating observable sensitive to sea ice thickness from the waveforms using (30) and (32);
4) estimate the amplitude and frequency of the oscillating observable using (31);
5) retrieve sea ice thickness using the retrieval model expressed by (33);
6) compare retrieved sea ice thickness with the truth.

Fig. 19 gives the comparison between the truth and retrieved sea ice thickness. Compared to the phase compensation method, the dual-polarization observations could obtain better performance. The main reason is that the dual-polarization observations more precisely compensate the delay phase between the direct and the reflected signal so that obtain a clearer oscillating pattern. The frequency of the oscillating pattern provides higher retrieving precision than that using the amplitude of the oscillating pattern. The reason is that the frequency of the oscillating pattern has a linear relationship as shown in Fig. 14, however, the amplitude has the inversely proportional relationship which causes a decreasing retrieval performance with increasing sea ice thickness, and fails to work when sea ice thickness is below 1 m. In addition, the partial estimations do clearly not agree with the truths, which are caused by the failed fitting. To evaluate this inconsistency between the retrieved value and truthes, the efficiency ratio is defined as

$$\eta = \frac{N_{\text{eff}}}{N_{\text{total}}} \times 100\% \tag{34}$$

where N_{eff} is the number of the effective retrievals for which the error is below 0.5 m and N_{total} is the simulation number. As given in Table II, for the phase compensation, the efficiency
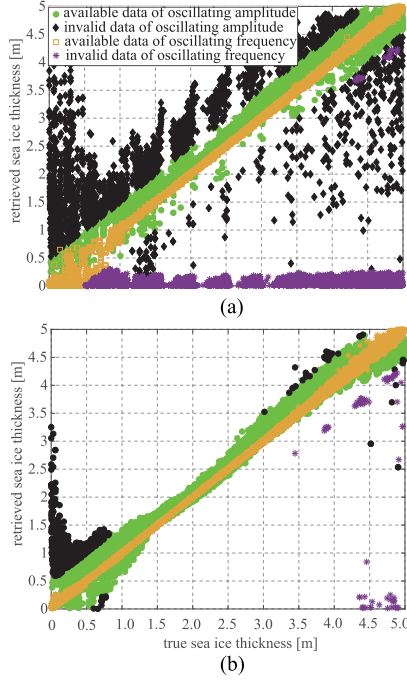
Fig. 19. Scatter between the truths and the retrieved sea ice thickness using (a) the phase compensation and (b) dual-polarization observations for the simulated data of the scenario given in Table I.

TABLE II
PARAMETERS OF SIMULATED SCENARIO

	efficiency [%]	RMSE [m]
amplitude of phase compensation	65.52	0.16
frequency of phase compensation	67.85	0.11
amplitude of dual-observation	94.21	0.16
frequency of dual-observation	95.54	0.03

ratios using the amplitude and the frequency of the oscillating pattern are 65.62% and 67.85%, respectively, and these of the dual-polarization observation are 94.21% and 95.54%, respectively. When using the oscillating amplitude and frequency of the phase-compensated pattern to retrieve sea ice thickness, the root-mean-square error (rmse) of 0.16 and 0.11 m are obtained. For the dual-polarization observation, the rmses using oscillating amplitude and frequency are 0.16 m and 0.03. This indicates that the dual-polarization observation more precisely corrects the delay phase so that obtain better retrieval performance, and among these defined observable the oscillating frequency of the dual-polarization observation provides the best retrieval result.

Fig. 20 shows the dependence of the rmses of the retrieved sea ice thickness on sea ice thickness for Monte Carlo simulation, in which all rmses experience concavely varying trends and show the best retrieval precision for the sea ice thickness from 2 to 3 m. When using the amplitude of the oscillating pattern, the low and high sea ice thickness have significantly worse results than the moderate sea ice thickness, due to the weaker sensitivity. The oscillating frequency of the phase compensation method presents worse precision than that using the oscillating frequency of the dual-polarization method for the low sea ice thickness. The main reason is that, as shown in Fig. 16, the retrieved height for low sea
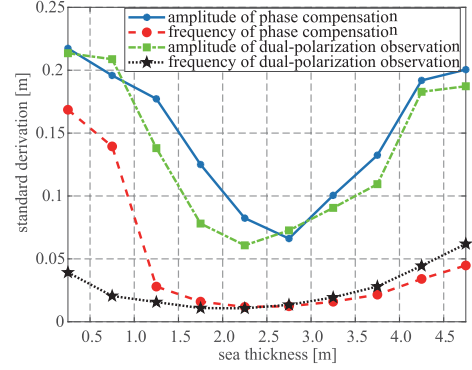

Fig. 20. RMSEs of the retrieved sea ice thickness for different sea ice thickness. The used data are simulated for the scenario in Table I.

ice thickness is wrong so that low accuracy compensation for the delay phase is obtained. To improve the retrieval performance, it is necessary to obtain a highly accurate reflector height.

VI. CONCLUSION

Sea ice detection and measurements near coastlines are important for climate monitoring and safe production. GNSS-R as a new bistatic remote sensing has been widely used to observe earth's physical parameters. Automatic detection and measurement of sea ice is becoming a promising application of coastal GNSS-R. At present, the methods to detect sea ice mainly are based on the amplitude or power of the reflected signals, such as the power ratio of the reflected and direct signal, and the polarimetric ratio of the reflected RHCP and LHCP signals. Because of the penetration of GNSS signal into sea ice, the signal components from the air–ice and ice–water interface interfere so that the amplitude or power experiences an oscillating pattern as a function of elevation angle. In addition, the gain modulation of the receiving antenna also has an influence on the amplitude or power of the reflected signal. The oscillation and the gain modulation would decrease the ability of detecting sea ice. To reduce these effects, suitable satellites have to be chosen to estimate the power ratio and polarimetric ratio.

Compared to an ice-free sea, a sea ice surface is smoother so that the signals reflected off a sea ice surface contain more coherent components than the signals reflected off the ice-free sea. Based on this, this article explored to use the phase coherency of the reflected signal to detect sea ice. In this article, two metrics including the correlation time and a random walk test were used to distinguish between sea water and sea ice. The correlation time for sea ice is larger than that of sea water, and compared to the signals reflected off the ice-free sea, the phases of the signals reflected off sea ice are less random. This indicates that the phase coherency is able to distinguish sea ice and sea water.

Sea ice thickness is an important parameters for climate monitoring and safe production, therefore, sea ice thickness measurement is a key in sea ice remote sensing. Limited work has been done for measuring sea ice thickness using GNSS-R. Based on the developed three-layer reflection model, it has been found that the oscillating amplitude and frequency of the

reflection coefficient's phase depend on sea ice thickness. This article explored the potential of the oscillating phase pattern in retrieving sea ice thickness. To obtain the phase pattern of the reflection coefficient from the reflected signal, it is necessary to remove the delay phase between the reflected and the direct signal from the estimated phase of reflected signal. For this purpose, two methods including the phase compensation method and the dual-polarization observation were proposed. The capacity of GNSS-R retrieving height could be used for the phase compensation method. The amplitude and frequency of the oscillating pattern were defined to measure sea ice thickness. When sea ice thickness is below 1 m, the oscillation amplitude of the oscillating pattern is steady around 1, and is inversely proportional with the sea ice thickness from 1 to 5 m. The frequency of the oscillating pattern showed a linear relationship with sea ice thickness. For the sea ice thickness below 1 m, due to the large error in retrieved reflector height using GNSS-R altimetry, the precision of the phase compensation is low so that it is difficult to accurately measure sea ice thickness. Compared to the phase compensation method, the dual-polarization observation provided a better performance with rmses of 0.16 and 0.11 m, and the efficiency ratio of 94.21% and 95.54% when using the oscillating amplitude and frequency. Finally, other factors influencing sea ice thickness were analyzed. The results showed that, when using the amplitude of the oscillating pattern to retrieve sea ice thickness, sea ice temperature has a weak influence on retrieving thick sea ice, and sea water temperature and salinity both have no significant impact. It was concluded that it is possible to retrieve sea ice thickness using the phase pattern of the reflected GNSS for coastal GNSS-R, and the frequency of the oscillating phase pattern is a better choice than the oscillating amplitude to retrieve sea ice thickness.

A limitation to measure sea ice thickness using the proposed methods are signal coherence. Although GNSS signals reflected off sea ice are more coherent than these reflected off a sea surface. When sea ice roughness exceeds a particular value, the coherence of the reflected signals could be lost. Therefore, sea ice roughness will determine the measurement ability. In [23], through analyzing TDS-1 data, the delay and Doppler waveforms from multiyear ice have shown slower decay from the maximum value than these from young and first-year ice. In [14], it was also found that the gradual ageing of sea ice has a weak correlation with increasing GPS-derived roughness. These indicate that compared to young and first-year ice, multiyear ice contains rougher ice structures so that the proposed method may have worse performance for multiyear sea ice than young and first-year ice. The penetration depth is other factor impacting the proposed methods. The increasing of sea ice thickness or water content in sea ice both decreases the components reflected off the ice–water inference, and results in the reduced ability of retrieving sea ice thickness. This indicates that when sea ice melts, sea ice thickness measurement will probably be impossible due to reduced penetration depth. In addition, different sea concentrations result in different reflection coefficients so that it is still difficult to simultaneously retrieve sea ice thickness and concentration.

The drawback of this article is that the experimental data used in this article are intermittently acquired every 30 min and each dataset contains about 50 s of the direct and reflected GNSS signals, therefore, the proposed methods for retrieving sea ice thickness are not demonstrated using experimental data. The proposed methods skillfully use the oscillating interference pattern as a function of elevation angle. In [25], the oscillating pattern of the signal reflected off sea ice surface has been investigated to retrieve snow and ice thickness. The interference pattern between the signals reflected off the air–ice and ice–water interface have also been found in other works, such as radiometry [51] and GNSS-IR [52], [53]. These works all indicated that the interference pattern of the signals reflected off an ice slab has the potential to retrieve sea ice thickness. The drawback of the experiment is expected to overcome in future.

APPENDIX A
REFLECTION COEFFICIENT OF THREE-LAYER MEDIUM

The RHCP electromagnetic wave is expressed by vertical and horizontal polarization as

$$\mathbf{E}_R = \frac{\mathbf{E}_\perp + \mathbf{E}_\parallel}{2} \tag{35}$$

where $\mathbf{E}_\perp$ and $\mathbf{E}_\parallel$ are the vertical and horizontal polarization electromagnetic wave. Correspondingly, the LHCP one is expressed as

$$\mathbf{E}_L = \frac{\mathbf{E}_\perp - \mathbf{E}_\parallel}{2}. \tag{36}$$

The vertical and horizontal incidence wave at point O are, respectively, expressed as

$$\mathbf{E}_\perp = \mathbf{i}_y E_0 \tag{37}$$

$$\mathbf{E}_\parallel = j \left(\mathbf{i}_x \cos\theta_0 - \mathbf{i}_z \sin\theta_0 \right) E_0. \tag{38}$$

Correspondingly, the reflected waves at point O in Fig. 1 are

$$\mathbf{E}_{r\perp 01} = \mathbf{i}_y \Gamma_{\perp 01} E_0 \tag{39}$$

$$\mathbf{E}_{r\parallel 01} = j \left(-\mathbf{i}_x \cos\theta_0 + \mathbf{i}_z \sin\theta_0 \right) \Gamma_{\parallel 01} E_0. \tag{40}$$

The vertical and horizontal incidence wave at point S are, respectively, expressed as

$$\mathbf{E}_{S\perp} = \mathbf{i}_y E_0 e^{j 2 k_{\text{air}} h_{\text{ice}} \tan\theta_1 \sin\theta_0} \tag{41}$$

$$\mathbf{E}_{S\parallel} = j \left(\mathbf{i}_x \cos\theta_0 - \mathbf{i}_z \sin\theta_0 \right) E_0 e^{j 2 k_{\text{air}} h_{\text{ice}} \tan\theta_1 \sin\theta_0}. \tag{42}$$

Correspondingly, the transmissive waves at point S are

$$\mathbf{E}_{t\perp 01} = \mathbf{i}_y T_{\perp 01} \mathbf{E}_{S\perp} \tag{43}$$

$$\mathbf{E}_{t\parallel 01} = j \left(\mathbf{i}_x \cos\theta_1 - \mathbf{i}_z \sin\theta_1 \right) T_{\parallel 01} \mathbf{E}_{t\parallel 01}. \tag{44}$$

The transmissive waves penetrate sea ice to the ice–water interface, two waves are expressed as

$$\mathbf{E}_{i\perp 12} = \mathbf{i}_y T_{\perp 01} \mathbf{E}_{S\perp} e^{-jk_{\mathrm{ice}}\frac{h_{\mathrm{ice}}}{\cos\theta_1}} \tag{45}$$

$$\mathbf{E}_{i\parallel 12} = j\left(\mathbf{i}_x \cos\theta_1 - \mathbf{i}_z \sin\theta_1\right) T_{\parallel 01} \mathbf{E}_{S\parallel} e^{-jk_{\mathrm{ice}}\frac{h_{\mathrm{ice}}}{\cos\theta_1}}. \tag{46}$$

The reflected waves for the vertical and horizontal polarization at point $S1$ are expressed as

$$\mathbf{E}_{i\perp 12} = \mathbf{i}_y \Gamma_{\perp 12} \mathbf{E}_{i\perp 12} \tag{47}$$

$$\mathbf{E}_{i\parallel 12} = j\left(-\mathbf{i}_x \cos\theta_1 - \mathbf{i}_z \sin\theta_1\right) \Gamma_{\parallel 12} \mathbf{E}_{i\parallel 12}. \tag{48}$$

The reflected waves penetrate the sea ice to the point O on the air–ice interface. And then two waves transmit to the air and are expressed as

$$\mathbf{E}_{t\perp 10} = \mathbf{i}_y T_{\perp 10} \mathbf{E}_{i\perp 12} e^{-jk_{\mathrm{ice}}\frac{h_{\mathrm{ice}}}{\cos\theta_1}} \tag{49}$$

$$\mathbf{E}_{t\parallel 10} = j\left(-\mathbf{i}_x \cos\theta_0 + \mathbf{i}_z \sin\theta_0\right) T_{\parallel 10} \mathbf{E}_{i\parallel 12} e^{-jk_{\mathrm{ice}}\frac{h_{\mathrm{ice}}}{\cos\theta_1}}. \tag{50}$$

Total reflected waves for vertical and horizontal polarization are the coherent superposition of the wave component from the air–ice and ice–water interface as

$$\mathbf{E}_{r\perp} = \mathbf{E}_{r\perp 01} + \mathbf{E}_{t\perp 10} = \mathbf{i}_y \Gamma_\perp E_0 \tag{51}$$

$$\mathbf{E}_{r\parallel} = \mathbf{E}_{r\parallel 01} + \mathbf{E}_{t\parallel 10}$$

$$= j\left(-\mathbf{i}_x \cos\theta_0 + \mathbf{i}_z \sin\theta_0\right) \Gamma_\parallel E_0 \tag{52}$$

where $\Gamma_\perp$ and $\Gamma_\parallel$ are

$$\Gamma_\perp = \Gamma_{\parallel 01} + T_{\parallel 10} \Gamma_{\parallel 12} T_{\parallel 01} e^{j2h_{\mathrm{ice}}\left(k_{\mathrm{air}}\cdot\sin\theta_1\sin\theta_0 - \frac{k_{\mathrm{ice}}}{\cos\theta_1}\right)} \tag{53}$$

$$\Gamma_\parallel = \Gamma_{\perp 01} + T_{\perp 10} \Gamma_{\perp 12} T_{\perp 01} e^{j2h_{\mathrm{ice}}\left(k_{\mathrm{air}}\cdot\sin\theta_1\sin\theta_0 - \frac{k_{\mathrm{ice}}}{\cos\theta_1}\right)}. \tag{54}$$

The total wave reflected to the air is expressed as

$$\mathbf{E}_{\mathrm{total}} = \mathbf{E}_{r\perp} + \mathbf{E}_{r\parallel} = \Gamma_R \mathbf{E}_R + \Gamma_L \mathbf{E}_L \tag{55}$$

where Γ_R and Γ_L, respectively, are

$$\Gamma_R = \frac{\Gamma_\perp + \Gamma_\parallel}{2} = \Gamma_{R01} + \Gamma_{R12} e^{j2h_{\mathrm{ice}}\alpha} \tag{56}$$

$$\Gamma_L = \frac{\Gamma_\perp - \Gamma_\parallel}{2} = \Gamma_{L01} - \Gamma_{L12} e^{j2h_{\mathrm{ice}}\alpha} \tag{57}$$

where $\Gamma_{R(L)01}$, $\Gamma_{R(L)12}$, and α has been given by (6)–(8). $\mathbf{E}_R$ and $\mathbf{E}_L$ are expressed as

$$\mathbf{E}_R = \left[\mathbf{i}_y + \left(-\mathbf{i}_x \cos\theta_0 + \mathbf{i}_z \sin\theta_0\right)\right] E_0 \tag{58}$$

$$\mathbf{E}_L = \left[\mathbf{i}_y - \left(-\mathbf{i}_x \cos\theta_0 + \mathbf{i}_z \sin\theta_0\right)\right] E_0. \tag{59}$$

REFERENCES

[1] S. M. Pershin et al., "Ice thickness measurements by Raman scattering," *Opt. Lett.*, vol. 39, no. 9, pp. 2573–2575, 2014.

[2] J. Karvonen, M. Simila, and M. Makynen, "Open water detection from Baltic sea ice Radarsat-1 SAR imagery," *IEEE Geosci. Remote Sens. Lett.*, vol. 2, no. 3, pp. 275–279, Jul. 2005.

[3] J. C. Comiso, D. J. Cavalieri, and T. Markus, "Sea ice concentration, ice temperature, and snow depth using AMSR-E data," *IEEE Trans. Geosci. Remote Sens.*, vol. 41, no. 2, pp. 243–252, Feb. 2003.

[4] T. Armitage and A. L. Ridout, "Arctic sea ice freeboard from AltiKa and comparison with CryoSat-2 and Operation IceBridge," *Geophys. Res. Lett.*, vol. 42, no. 16, pp. 6724–6731, 2015.

[5] L. A. Breivik, S. Eastwood, and T. Lavergne, "Use of C-band Scatterometer for sea ice edge identification," *IEEE Trans. Geosci. Remote Sens.*, vol. 50, no. 7, pp. 2669–2677, Jul. 2012.

[6] C. Hall and R. Cordey, "Multistatic Scatterometry," in *Proc. Int. Geosci. Remote Sens. Symp., 'Remote Sens.: Moving Toward 21st Century*, 1988, pp. 561–562.

[7] M. Martin-Neira, "A passive reflectometry and interferometry system (PARIS): Application to ocean altimetry," *ESA J.-Eur. Space Agency*, vol. 17, no. 4, pp. 331–355, 1993.

[8] M. P. Clarizia, C. Ruf, P. Cipollini, and C. Zuffada, "First spaceborne observation of sea surface height using GPS-reflectometry," *Geophys. Res. Lett.*, vol. 43, no. 2, pp. 767–774, Jan. 2016.

[9] G. Foti et al., "Spaceborne GNSS reflectometry for ocean winds: First results from the UK TechDemoSat-1 mission," *Geophysical Res. Lett.*, vol. 43, no. 2, pp. 767–774, 2015.

[10] S. J. Katzberg, O. Torres, M. S. Grant, and D. Nasters, "Utilizing calibrated GPS reflected signals to estimate soil reflectivity and dielectric constant: results from SMEX02," *Remote Sens. Environ.*, vol. 100, no. 1, pp. 17–28, 2006.

[11] A. Camps et al., "Sensitivity of GNSS-R spaceborne observations to soil moisture and vegetation," *IEEE J. Sel. Topics Appl. Earth Observ. Remote Sens.*, vol. 9, no. 10, pp. 4730–4742, Oct. 2016.

[12] A. Komjathy, J. Maslanik, and P. Axelrad, "Sea ice remote sensing using surface reflected GPS signals," in *Proc. Geosci. Remote Sens. Symp.*, 2000, pp. 2855–2857.

[13] M. Wiehl, B. Legresy, and R. Dietrich, "Potential of reflected GNSS signals for ice sheet remote sensing," *Prog. Electromagn. Res.*, vol. 40, pp. 177–205, 2003.

[14] M. B. Rivas, J. A. Maslanik, and P. Axelrad, "Bistatic scattering of GPS signals off Arctic Sea ice," *IEEE Trans. Geosci. Remote Sens.*, vol. 48, no. 3, pp. 1548–1553, Mar. 2010.

[15] S. Gleason, "Remote sensing of ocean, ice and land surfaces using bistatically scattered GNSS signals from low earth orbit," Ph.D. dissertation, Univ. Surrey, Guildford, U.K., 2006.

[16] Q. Yan and W. Huang, "Spaceborne GNSS-R Sea ice detection using delay-doppler maps: first results from the U. K. TechDemoSat-1 mission," *IEEE J. Sel. Topics Appl. Earth Observ. Remote Sens.*, vol. 9, no. 10, pp. 4795–4801, Oct. 2016.

[17] A. Alonso-Arroyo, V. U. Zavorootny, and A. Camps, "Sea ice detection using U.K. TDS-1 GNSS-R data," *IEEE Trans. Geosci. Remote Sens.*, vol. 55, no. 9, pp. 3782–3788, Sep. 2017.

[18] Q. Yan, W. Huang, and C. Moloney, "Neural networks based sea ice detection and concentration retrieval from GNSS-R delay-doppler maps," *IEEE J. Sel. Topics Appl. Earth Observ. Remote Sens.*, vol. 10, no. 8, pp. 3789–3798, Aug. 2017.

[19] Y. Zhu, T. Tao, J. Zou, K. Yu, J. Wickert, and M. Semmling, "Spaceborne GNSS reflectometry for retrieving sea ice concentration using TDS-1 data," *IEEE Geosci. Remote Sens. Lett.*, vol. 18, no. 4, pp. 612–616, Apr. 2021.

[20] A. Rius et al., "Feasibility of GNSS-R ice sheet altimetry in greenland using TDS-1," *Remote Sens.*, vol. 9, no. 7, 2017, Art. no. 742.

[21] W. Li et al., "First spaceborne phase altimetry over sea ice using TechDemoSat-1 GNSS-R signals," *Geophys. Res. Lett.*, vol. 44, no. 16, pp. 8369–8376, 2017.

[22] Q. Yan and W. Huang, "Sea ice thickness measurement using spaceborne GNSS-R: First results with TechDemoSat-1 data," *IEEE J. Sel. Topics Appl. Earth Observ. Remote Sens.*, vol. 13, pp. 577–587, 2020.

[23] N. Rodriguez-Alvarez et al., "An Arctic Sea ice multi-step classification based on GNSS-R data from the TDS-1 mission," *Remote Sens. Environ.*, vol. 230, 2019, Art. no. 111202.

[24] W. Li et al., "Measuring Greenland ice sheet melt using spaceborne GNSS reflectometry from TechDemoSat-1," *Geophys. Res. Lett.*, vol. 47, 2020, Art. no. e2019GL086477.

[25] J. F. Munoz-Martin et al., "Snow and ice thickness retrievals using GNSS-R: Preliminary results of the MOSAiC experimental," *Remote Sens.*, vol. 12, 2020, Art. no. 4038.

[26] F. Fabra et al., "Monitoring sea-ice and dry snow with GNSS reflections," in *Proc. IEEE Int. Geosci. Remote Sens. Symp.*, Honolulu, HI, USA, 2010, pp. 3837–3840.

[27] Z. Yun et al., "Detection of Bohai Bay Sea ice using GPS-reflected signals," *IEEE J. Sel. Topics Appl. Earth Observ. Remote Sens.*, vol. 8, no. 1, pp. 39–46, Jan. 2015.

[28] J. Strandberg, T. Hobiger, and R. Haas, "Coastal Sea ice detection using ground-based GNSS-R," *IEEE Geosci. Remote Sens. Lett.*, vol. 14, no. 9, pp. 1552–1556, Sep. 2017.

[29] F. Fabra *et al.*, "Phase altimetry with dual polarization GNSS-R over sea ice," *IEEE Trans. Geosci. Remote Sens.*, vol. 50, no. 6, pp. 2112–2121, Jun. 2012.

[30] H. Gao, D. Yang, and Q. Wang, "Retrieval of sea ice thickness using global navigation satellite system reflected signals," *Meas. Control*, vol. 52, pp. 7–8, 2019.

[31] Y. Zhang *et al.*, "Sea ice thickness detection using coastal BeiDou reflection setup in Bohai Bay," *IEEE Geosci. Remote Sens. Lett.*, vol. 18, no. 3, pp. 381–385, Mar. 2021.

[32] L. A. Klein and C. T. Swift, "An improved model for the dielectric constant of sea water at microwave frequencies," *IEEE J. Ocean. Eng.*, vol. 2, no. 1, pp. 104–111, Jan. 1977.

[33] D. Frank, *Microwave Remote Sensing of Sea Ice-The Physical Basis for Sea Ice Remote Sensing*. Washington, DC, USA: American Geophysical Union, 1992.

[34] F. T. Ulaby, R. K. Moore, and A. K. Fung, *Microwave Remote Sensing: Active and Passive*. Reading, MA, USA: Addison-Wesley, 1982, pp. 2044–2048.

[35] G. F. N. Cox and W. F. Weeks, "Numerical simulations of the profile properties of undeformed first-year sea ice during the growth season," *J. Geophy. Res.*, vol. 93, pp. 12449–12460, 1988.

[36] J. A. Edminiser, *Theory and Problems of Electromagnetics*. New York, NY, USA: McGraw-Hill, 1986.

[37] E. Cardellach *et al.*, "Characterization of dry-snow sub-structure using GNSS reflected signals," *Remote Sens. Environ.*, vol. 124, no. 1, pp. 122–134, 2012.

[38] V. U. Zavorotny and A. G. Voronovich, "Scattering of GPS signals from the ocean with wind remote sensing application," *IEEE Trans. Geosci. Remote Sens.*, vol. 38, no. 2, pp. 951–964, Mar. 2000.

[39] F. Soulat *et al.*, "Sea state monitoring using coastal GNSS-R," *Geophys. Res. Lett.*, vol. 31, no. 21, pp. 133–147, 2004.

[40] F. Wang, D. Yang, B. Zhang, W. Li, and J. Darrozes, "Wind speed retrieval using coastal ocean-scattered GNSS signals," *IEEE J. Sel. Topics Appl. Earth Observ. Remote Sens.*, vol. 9, no. 11, pp. 5272–5283, Nov. 2016.

[41] E. Valencia, A. Camps, J. F. Marchan-Hernandez, N. Rodriguez-Alvarez, I. Ramos-Perez, and X. Bosch-Lluis, "Experimental determination of the sea correlation time using GNSS-R coherent data," *IEEE Geosci. Remote Sens. Lett.*, vol. 7, no. 4, pp. 675–679, Oct. 2010.

[42] M. M. Al-Khaldi, R. Shah, C. C. Chew, J. T. Johnson, and S. Gleason, "Mapping the dynamics of the south asian monsoon using CYGNSS's level-1 signal coherency," *IEEE J. Sel. Topics Appl. Earth Observ. Remote Sens.*, vol. 14, pp. 1111–1119, 2021.

[43] A. Alonso-Arroyo, A. Camps, H. Park, D. Pascual, R. Onrubia, and F. Martín, "Retrieval of significant wave height and mean sea surface level using the GNSS-R interference pattern technique: Results from a three-month field campaign," *IEEE Trans. Geosci. Remote Sens.*, vol. 53, no. 6, pp. 3198–3209, Jun. 2015.

[44] J. Strandberg, T. Hobiger, and R. Hass, "Improving GNSS-R sea level determination through inversemodeling of SNR data," *Radio Sci.*, vol. 51, pp. 1286–1296, 2016.

[45] A. M. Semmling *et al.*, "Detection of Arctic Ocean tides using interferometric GNSS-R signals," *Geophys. Res. Lett.*, vol. 38, no. 4, 2011, Art. no. L04103.

[46] G. Ruffini and F. Soulat, "On the GNSS-R interferometric complex field coherence time," Starlab, Barcelona, Spain, Tech. Brief 0005, 2004.

[47] S. Gleason, C. Gommenginger, and D. Cromwell, "Fading statistics and sensing accuracy of ocean scattered GNSS and altimetry signals," *Adv. Space Res.*, vol. 46, no. 2, pp. 208–220, 2010.

[48] J. D. Gibbons, and S. Chakraborti. *Nonparametric Statistical Inference*, 5th ed. Boca Raton, FL, USA: CRC Press, 2011.

[49] A. Camps, "Spatial resolution in GNSS-R under coherent scattering," *IEEE Geosci. Remote Sens. Lett.*, vol. 17, no. 1, pp. 32–36, Jan. 2020.

[50] J. T. Vanderplas, "Understanding the Lomb-Scargle periodogram," *Astrophys. J. Suppl. Ser.*, vol. 236, no. 16, pp. 1–28, 2018.

[51] L. Kaleschke, N. Maaß, and C. Haas, "A sea-ice thickness retrieval model for 1.4 GHz radiometry and application to airborne measurement over low salinity sea," *Gryosphere*, vol. 4, pp. 583–592, 2010.

[52] Q. Chen, D. Won, and D. M. Akos, "Snow depth estimation accuracy using a dual-interface GPS-IR model with experimental results," *GPS Solutions*, vol. 21, pp. 211–223, 2017.

[53] M. D. Jacobson, "Potential for estimating the thickness of freshwater lake ice by GPS interferometric reflectometry," *J. Geography Geol.*, vol. 7, pp. 10–19, 2015.

Feng Wang received the bachelor's degree in electronic and information engineering from the School of Electronic and Information Engineering, the master's degree in communication and information engineering, and the Ph.D. degree in information and signal processing from Beihang University, Beijing, China, in 2012, 2014, and 2019, respectively.

He started his Postdoctoral work with the School of Electronic and Information Engineering, Beihang University, in 2020. His research interest includes global navigation satellite system reflectometry (GNSS-R) application in ocean observation.

Dongkai Yang was born in China in 1972. He received the B.S. degree in electronic engineering from the North University of China, Taiyuan, China, in 1994, and the M.S. and Ph.D degrees in communication and information system from Beihang University, Beijing, China, in 1997 and 2000, respectively.

From 2001 to 2002, he was a Research Fellow with the Nanyang Technological University, Singapore. Since 2010, he has been a Full Professor with the School of Electronic and Information Engineering, Beihang University. His interests include global navigation satellite system and its application.

Mingjie Niu received the bachelor's degree in electronic and information engineering from the School of Electrical and Electronic Engineering, North China Electric Power University, Beijing, China, in 2019. He is currently working toward the master's degree in communication and information engineering with the School of Electronic and Information Engineering, Beihang University, Beijing, China.

His research interest includes global navigation satellite system reflectometry application in ocean observation.

Lei Yang was born in China in 1972. He received the B.S. and M.S. degrees in computer science from Northwest Polytechnical University, Xian, China, in 2004 and 2008, respectively, and the Ph.D. degree in agricultural electrification and automation from Shandong Agricultural University, Taian, China, in 2017.

Since 2012, he has been a Lecturer with the School of Information Science and Technology, Shandong Agricultural University. His current research interests include GNSS-R and ASIC design.

Bo Zhang received the Ph.D. degree in communication and information engineering from the School of Electronic and Information Engineering, Beihang University, Beijing, China, in 2006.

From 2006 to 2009, he has been a Postdoctoral of electronic science and technology with Beihang University, where he has been a Lecturer with the School of Electronic and Information Engineering, since 2009. His research interests include GNSS and spread spectrum communication.